参赛队员姓名：丁冠文 夏锐涵 杨博约

中学：南京外国语学校

省份：江苏

国家/地区：中国/南部赛区

指导教师姓名：陈晓君、陈静

指导单位：南京工业大学、南京外国语学校

论文题目：基于核壳结构沸石咪唑盐框架结构构建新型电化学适配体传感器检测赭曲霉毒素 A

基于核壳结构沸石咪唑盐框架结构构建新型电化学适配体传感器检测赭曲霉毒素 A

丁冠文 夏锐涵 杨博约

南京外国语学校，江苏南京 210018

摘 要：赭曲霉毒素 A（OTA）是一种主要由青霉菌和曲霉菌分泌的有害真菌毒素。本文构建了一种基于核壳型沸石咪唑盐框架材料（ZIFs）ZIF-8@ZIF-67 传感平台和双特异性核酸酶（DSN）引发杂交链反应（HCR）信号放大策略的电化学 OTA 适配体传感器。以金纳米粒子（AuNPs）植入 ZIF-8@ZIF-67（AuNPs/ZIF-8@ZIF-67）作为纳米载体，修饰在氧化铟锡（ITO）玻璃电极表面，用于固载巯基化发夹探针（HP1）。当待测体系中没有 OTA 时，RNA 链打开发夹适配体（HP）形成 DNA/RNA 异质双链，其中在 DNA 链的一端有一段不匹配的单链 DNA（ssDNA）。DSN 能够选择性地在双链中剪切 DNA 链并释放 RNA，释放的 RNA 会引发更多的 DSN 反应周期。同时释放出来 ssDNA 与电极表面固定的 HP1 结合，并且启动 HCR 反应，形成了纳米线结构。在纳米线上自发形成了 G-四链体/血红素复合物，在溶液中含有烟酰胺腺嘌呤二核苷酸（NADH）时，以硫堇分子（Thi）作为氧化还原探针，可产生放大的电化学响应信号。然而，在 OTA 存在的情况下，HP 与 OTA 之间高亲和性结合导致部分 HP 不能与 RNA 杂交，因此 ssDNA 的释放量减少，使得 DPV 法检测到 Thi 的电化学信号降低。在最优实验条件下，该传感器对 OTA 的线性响应范围为 0.1-10 $ng \cdot mL^{-1}$，检测限为 0.247 $fg \cdot mL^{-1}$。而且，在实际小麦样品中检测回收率为 96.8-104.2%，显示了该传感器广阔的应用前景。

关键词：沸石咪唑盐框架材料；核壳型结构；电化学适配体传感器；赭曲霉毒素 A；信号放大策略

Ultrasensitive detection of ochratoxin A with a novel electrochemical aptasensor based on core-shell zeolite imidazolate frameworks

Guanwen Ding, Ruihan xia, Boyue Yang

Nanjing Foreign Language School, Nanjing 210018, PR China

Abstract: Ochratoxin A (OTA) is a harmful mycotoxin which is mainly secreted by Penicillium and Aspergillus species. In this work, an electrochemical aptasensor is presented for OTA detection based on core-shell zeolite imidazolate frameworks (ZIFs) ZIF-8@ZIF-67 platform and duplex-specific nuclease (DSN) triggered hybridization chain reaction (HCR) signal amplification. The surface of indium tin oxide (ITO) coated glass electrode was modified with Au nanoparticles (AuNPs) implanted ZIF-8@ZIF-67 (AuNPs/ZIF-8@ZIF-67) as nanocarrier for the immobilization of thiolated hairpin (HP1). In the absence of OTA, RNA strand opened hairpin aptamer (HP) to form DNA/RNA heteroduplex, which had an unmatched single-stranded DNA (ssDNA) on one end. DSN was able to shear DNA strand in the duplex and release RNA to trigger more cycles of DSN reaction. Unmatched ssDNA was exposed to open HP1 assembled on the electrode and initiate HCR to form G-quadruplex-hemin DNAzyme. Besides, thionine (Thi) was enriched as a redox probe for signal amplification with the help of nicotinamide adenine dinucleotide (NADH). Otherwise, in the presence of OTA, the high affinity between HP and OTA caused a part of HP could not hybridize with RNA, thus the decrease in the amount of released ssDNA obtained a decreased electrochemical signal from Thi detected by DPV method. With the optimal experimental parameters, the linear response range was from 0.1 fg·mL^{-1} to 10 ng·mL^{-1}, and the detection limit was estimated as 0.247 fg·mL^{-1}. Furthermore, the aptasensor was proven to be applied in real wheat samples with a recovery between 96.8% and 104.2%, illustrating the potential prospects in practical detection.

Keywords: Zeolite imidazolate frameworks; core-shell structure; electrochemical aptasensor; ochratoxin A; signal amplification strategy.

Content

1. Introduction

Ochratoxin is a kind of toxic secondary metabolites produced by ochra and penicillium fungi, which includes seven types of homologous structure compounds. Ochratoxin A (OTA) is known as the most toxic type and classified as Level 2B carcinogen by the International Agency of Research on Cancer [1]. It can threat the health of most mammalian species in liver, kidneys and immune system. OTA contamination can be found in a wide range of food products, such as cereals, beans, coffee, wine, animal meat, nuts, etc [2]. Besides, OTA is highly stable in chemical and thermal circumstances, so it is quite stable in products even after long-time storage and is difficult to be fully removed in the course of food manufacturing process [3]. Hence, OTA can even be found in people's body since they eat the contaminated food [4]. Due to its potential toxicity, some regulatory agencies of the European Union have introduced the maximum level of OTA in food stuff (5 or 10 $\mu g \cdot kg^{-1}$) and beverages (2 $\mu g \cdot kg^{-1}$) (EC No. 123/2005). In general, the concentration of OTA is pretty low in the early stage of food processing. Hence, it is urgent to develop highly sensitive methods for the detection of trace OTA in food.

Up to now, many instrumental analytical methods have been reported for OTA detection, including high-performance liquid chromatography (HPLC), HPLC-fluorescence detector (HPLC-FLD), liquid chromatography tandem mass spectrometry (LC-MS/MS), thin layer chromatography (TLC), enzyme-linked immunosorbent assay (ELISA) and immunochromatographic assay (ICA) [5-10]. Although these chromatography and immunoassays have good sensitivity, high selectivity and stability, they are limited to high-cost expenses, complicated operation requirements and strict experimental conditions, and not suitable to extend for the field testing. Therefore, developing a high sensitivity and low cost strategy for OTA detection is of great significant for universal application. Compared with the aforementioned methods, the electrochemical methods have the advantages of simple operation, low cost, fast response, excellent compatibility with miniaturization

technologies and easy on-site detection. Thereinto, various electrochemical biosensors for OTA have arisen, mainly involving immunosensors, capacitance biosensors, photo-electrochromic biosensors, aptasensors, etc [11-14]. Among them, the electrochemical aptasensors have been attracted more and more attentions since they combine the advantages of electrochemical methods and aptamers.

As a powerful alternative to antibodies, aptamers hold the favorable advantages of simpler production, higher affinity and specificity together with a better stability and commercially availability [15,16]. Ever since the first time reported that the aptamer was applied for OTA detection by Cruz-Aguado's team [17], diverse OTA electrochemical aptasensors have been widely introduced. Hairpin-DNA aptamer towards OTA was firstly reported by Zhang et al. with a linear response concentration range from 1.0 to 20 $pg \cdot mL^{-1}$ [18]. In a recent work, based on aptamer/NH_2 Janus particles, an ultrasensitive OTA aptasensor exhibited a wide dynamic range of 1×10^{-5}-10 nM with an ideal performance of OTA detection in red wine samples [19]. Although these systems were sensitive for OTA detection, development of novel aptasensors with different principles is still required.

To further make the best use of electrochemical aptasensors, electrode materials are crucial to enhance the sensitivity and stability. A variety of nanomaterials with good biocompatibility and electron transfer capability have been used as carrier or platform to amplify the electrochemical sensing signals, including metal nanopaticles, metal oxides, carbon-based nanostructures, and other nanocomposites [20]. Metal-organic frameworks (MOFs) are a rising class of highly porous hybrid materials, which have exhibited prospective applications in catalysis, storage and separation, gas absorption and drug delivery [21]. However, MOFs participating in the construction of electrochemical aptasensors is limited by their unfavorable conductivity and electroactivity. Therefore, various MOFs composites with metal nanoparticles, carbon nanostructures and conductive polymers have been assembled for a wide application in electrochemical field [22]. In addition, zeolitic imidazolate framworks (ZIFs) is a novel series of MOFs, which combine the advantages of both MOFs and zeolite, exhibiting exceptional thermal and chemical stability of inorganic zeolite [23].

Because of the above-mentioned advantages, ZIFs composite was used as a carrier in this work to load biomaterials. At present, the exploration of ZIF-based aptasensors is still in its infancy [24,25], and significantly, there is no reports on ZIFs-based electrochemical aptasensors for OTA detection.

Recently, multi-metal ZIFs, especially with the core-shell nanostructures have attracted widespread attention due to their excellent physical and chemical properties, tunable channel structure, controllable nanoparticle size and well-defined morphology [26]. ZIF-8 [$Zn(Hmim)_2$] and ZIF-67 [$Co(Hmin)_2$] are two kinds of classic ZIFs, which have been extensively explored [27,28]. Since they belong to the same isostructure, the core-shell ZIF-8@ZIF-67 could be obtained by means of the epitaxial growth with ZIF-8 as seed [29]. The synergistic effects would be realized by the combining the respective advantages of the two single metal ZIFs, in which the large-sized shell ZIF-67 could facilitate the mass transfer onto the surface of core ZIF-8 [30]. In this way, the biosensing performance should be enhanced based on the ZIF-8@ZIF-67 nanocarrier.

With this idea in mind, a heterogeneous composite of Au nanoparticles (AuNPs)/ZIF-8@ZIF-67 was designed and synthesized in this work and served as a conductive platform for supporting and sensing, by implanting ultrafine AuNPs into the highly regular ZIF-8@ZIF-67. Moreover, the structure of ZIF-8@ZIF-67 can still remain intact after the composite with AuNPs. At the same time, in an attempt to boost the number of recycling oligonucleotides for signal amplification, duplex-specific nuclease (DSN) was adopted. It can identify and digest DNA strand from a DNA/RNA duplex, and then the released RNA could be recycled [31]. The schematic illustration of this work is shown in Scheme 1. In the absence of OTA, hairpin aptamer (HP) hybridized with RNA strand, which triggered DSN shearing reaction. A short strand named ssDNA could be produced, which initiated a hybridization chain reaction (HCR) on the AuNPs/ZIF-8@ZIF-67 modified electrode surface. The remained parts in HP2 and HP3 combined with Hemin molecules to form G-quadruplex-hemin DNAzymes. In the catalytic reaction, thionine (Thi) was adopted as a redox probe and nicotinamide adenine dinucleotide (NADH) worked as

coenzyme to further amplify the electrochemical signal [32]. In the presence of OTA, HP preferentially combined with OTA due to the high affinity between the aptamer and OTA. The RNA strands failed to release ssDNA and trigger the subsequent HCR reactions, and then a weaker redox signal was recorded in comparison with the signal in the absence of OTA. The quantitation of OTA therefore relied on the inversely linear relationship between OTA concentration (C_{OTA}) and current signal of Thi.

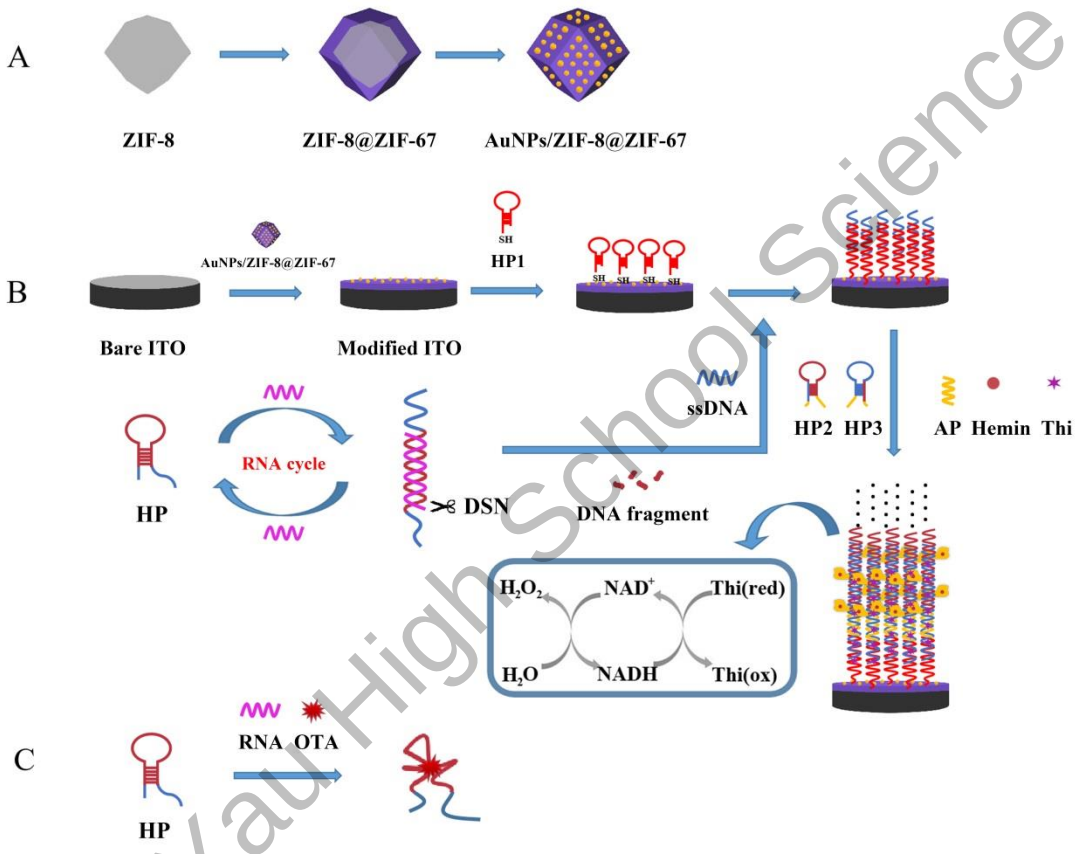

Scheme 1. Schematic illustration of the principle of the electrochemical aptasensor: (A) fabrication of the AuNPs/ZIF-8@ZIF-67, (B) DSN-assisted signal amplification strategy in the absence of OTA, and (C) selective recognition of HP with OTA.

2. Experimental

2.1 Materials and instrumentation

Cobalt (II) nitrate hexahydrate ($Co(NO_3)_2 \cdot 6H_2O$) and zinc(II) nitrate hexahydrate ($Zn(NO_3)_2 \cdot 6H_2O$) were purchased from Xilong Chemical Reagent (Guangdong, China). Sodium borohydride ($NaBH_4$) and 2-methyl imidazole (2-MI) were obtained from Aladdin (Shanghai, China). Methanol, acetone, absolute ethanol were purchased from Shanghai Linfeng Chemical Reagent (China). Chloroauric acid hydrated ($HAuCl_4 \cdot 4H_2O$) were purchased from Beijing HWRK Reagent (China). NADH, Thi, hexanethiol (96%, HT), hemin were obtained from Aldrich (Shanghai, China). Tris (2-carboxyethyl) phosphine hydrochloride (TCEP-HCl) was purchased from Baoman Biotech. Co. Ltd. (Shanghai, China). 0.1 M pH 7.0 PBS containing 5 mM $[Fe(CN)_6]^{3-/4-}$ was used for cyclic voltammetry (CV) and electrochemical impedance spectroscopy (EIS) experiments. Hemin solution was prepared by 0.15 mM hemin, 0.25 mM HEPES, 0.20 mM KCl, 2 mM NaCl and 1 mM DMSO. OTA was obtained from PriboLab (Qingdao, China). DSN and the buffer were purchased from Evrogen Joint Stock Company (Moscow, Russia). All functional group-modified oligonucleotides were synthesized and purified by Takara Biotechnology Co., Ltd. (Dalian, China) and Sangon Biotechnology Co., Ltd. (Shanghai, China). Indium tin oxide (ITO) coated glass slides (coating thickness 180 ± 25 nm, sheet resistance < 15 U/cm^2) were purchased from Kaivo Electronic Components Co., Ltd. (Zhuhai, China). All solutions used in this work were prepared with ultrapure water. All chemicals were analytical grade and used without further purification. The oligonucleotide sequences used in this work were listed in Table 1.

Table 1. Oligonucleotides used in this work

Oligonucleotide	Sequence (from 5′ to 3′)
HP	HS-C6-TTT TTT GAT CGG GTG TGG GTG GCG TAA AG G GAG CAT CGG ATC AAT CCG TCG AGC AGA GTT CC A TGT GTA GAT AGC TTA
HP1	HS-C6- CCA TGT GTA GAT CAG ACT ATT CGA TTA AG C TAT CTA CAC ATG G
HP2	AGG GCG GGT GGG TGT TTA AGT TGG AGA ATT GTA CTT AAA CAC CTT CTT CTT GGG T
HP3	TGG GTC AAT TCT CCA ACT TAA ACT AGA AGA AGG TGT TTA AGT TGG GTA GGG CGG G
AP	AAC TCT GCT CGA CGG ATT AGA AGA AGG TGT TTA AGT A
RNA	U CCG AUG CUC UUA CGC CAC CCA CAC CCG AUC

Note: The red font in HP is the OTA aptamer. Letters of the same color (blue, green and brown) are respectively complementary each other. The stem part in HP, HP1, HP2 and HP3 was marked with underlines.

Electrochemical measurements including differential pulse voltammetry (DPV), CV and EIS were conducted on CHI 660E electrochemical workstation (Chenhua Instrument, Shanghai, China) with a three-electrode system, consisting of a saturated calomel reference electrode (SCE), a platinum wire auxiliary electrode and a modified ITO working electrode. The morphology of the nanostructures was investigated by scanning electron microscopy (SEM, Zeiss Sigma 300) and transmission electron microscope (TEM, FEI Talos F200S). The X-ray diffraction (XRD) pattern of ZIF-8@ZIF-67 was recorded in the 2θ scan range from 5 to 40° using Cu kα radiation with wavelength (λ) of 0.154 nm. A Nicolet iS5 (Thermo Fisher Scientific, USA) Fourier transform infrared resonance (FTIR) instrument was used to record the FTIR spectra of the samples using KBr pellet method. The particle size of

ZIFs was measured by dynamic light scattering (DSL, NanoBrook omni) instrument from 0.3 nm to 10 μm. Elemental mapping, and energy dispersive spectrometer (EDS) were characterized on SEM (Hitachi S4800), and the corresponding TEM images were measured on JEOL JEM-200CX. Agarose gel electrophoresis (AGE) analysis was performed in 1×TAE buffer at a constant voltage of 120 V for 40 min at room temperature. 2 % agarose solution was used as the media of electrophoresis. After separation, the gel was stained with ethidium bromide (EB) and scanned using gel imaging system (Bio-Rad, Shanghai). The 50-500 bp DNA Ladder (Solarbio, Beijing) was applied as marker in the analysis of DNA bands.

2.2 Preparation of ZIF-8@ZIF-67

ZIF-8@ZIF-67 was prepared in two steps according to a previous literature [33]. At the first step, A 26 mg of $Zn(NO_3)_2 \cdot 6H_2O$ was pre-added to 100 mL methanol solution containing 0.1 M of 2-MI. After ultrasonic treatment for 10 min, the solution was mixed thoroughly with another 100 mL methanol solution containing 1.468 g $Zn(NO_3)_2 \cdot 6H_2O$ and let it stand at room temperature for 24 h. The precipitated ZIF-8 was washed with methanol for three times and vacuum-dried for 12 h at room temperature [34]. At the second step, 1.164 g $Co(NO_3)_2 \cdot 6H_2O$, 0.1 g ZIF-8 and 1.232 g 2-MI were dissolved or dispersed in 20 mL methanol, respectively. After forming homogeneous solution, Co^{2+} solution was added into ZIF-8 dispersion dropwise under stirring. Then, 2-MI solution was dropped into the above-prepared solution and kept stirring for 24 h at room temperature. The resulting light purple sediment was washed with methanol for three times and vacuum-dried for 12 h at room temperature for further use.

2.3 Preparation of AuNPs/ZIF-8@ZIF-67

AuNPs/ZIF-8@ZIF-67 was prepared according to a previous report [35]. 0.2 g of ZIF-8@ZIF-67 was added into 20 mL of 10 mM $HAuCl_4$ solution and stirred for 12 h at room temperature. Then, 10 mL of 0.2 M $NaBH_4$ solution was added and stirred for

another 30 min. The resulting AuNPs/ZIF-8@ZIF-67 was washed with water and dried under vacuum at 60 ℃ for 12 h.

2.4 Fabrication of AuNPs/ZIF-8@ZIF-67 modified electrode

Firstly, ITO electrode was successively cleaned with acetone, ethanol and distilled water, and then dried with nitrogen for further use. The electrode area was confined by bounding a 3-mm-diameter circular-opened insulating tape. Then, 10 μL of 1 $mg \cdot mL^{-1}$ AuNPs/ZIF-8@ZIF-67 dispersion was dropped onto the electrode surface and dried naturally under room ambience, which was designated as AuNPs/ZIF-8@ZIF-67/ITO and stored at 4 °C.

2.5 Process of the aptasensing

Before aptasensing, 20 μL of HP, HP1, HP2 or HP3 solution with concentration of 4 μM was heated and activated at 95 °C for 5 min and then cooled down to room temperature prior to use. Significantly, since HP and HP1 are -SH group modified, to reduce the formation of disulfide bond, per 100 μL of solution was added with 0.1 μL of 100 mM TCEP-HCl after activation. All DNA sequences were diluted with 0.1 M PBS (pH 7.0) and RNA sequence was diluted with TE buffer. 20 μL of different concentrations of HP1 was immersed on the AuNPs/ZIF-8@ZIF-67/ITO surface at room temperature for 2 h. In this procedure, thiolated HP1 bound to the electrode surface via Au-S bonding. After that, the electrode was rinsed with distilled water and then incubated with 0.25 wt% bovine serum albumin (BSA) solution for 30 min to block the residue active sites on electrode surface.

After that, the electrode was immersed in 20 μL of mixture (containing 7 μL of 2 μM HP, 1 μL of OTA with different concentrations, 1 μL of 10×DSN buffer, 1 μL of 2 μM RNA and 0.1 U DSN) and reacted at 50 °C for 30 min. This process was aimed at activating DSN and cleaving DNA-RNA duplex. Then, 10 μL of 2×DSN STOP solution was added for another 5 min. At this time, the released DNA had been digested and ssDNA had been generated. A part of HP1 strands on electrode surface could hybrid with ssDNA after incubating with the above mixture at room

temperature for 2 h. After thoroughly cleaning with PBS, the ssDNA/HP1/AuNPs/ZIF-8@ZIF-67/ITO electrode was incubated with 10 μL of mixture containing 1 μM HP2, 1 μM HP3, 1 μM AP, 0.25 mM Thi and 0.15 mM hemin to initiate HCR reaction [36]. After the incubation at room temperature for 2 h, the hemin/G-quadruplex was formed and acted as a horse radish peroxidase (HRP) mimicking enzyme for NADH oxidation with the aid of dissolved O_2. During this process, Thi worked as an electron mediator and a dramatically amplified current signal could be observed. DPV measurements were carried out in 10 mL PBS (pH 7.0) containing 3 mM NADH within the potential range from -0.4 to 0 V.

3. Results and discussion

3.1 Characterization of AuNPs/ZIF-8@ZIF-67

Surface functional groups and formation of zinc-cobalt nuclear imidazole coordination polymer were observed by FTIR spectra. As depicted in Figure 1A, both precursor ZIF-8 (curve b) and ZIF-8@ZIF-67 (curve c) showed a C=N stretching vibration at 600 cm^{-1} and a aliphatic C-H stretch at 3129 cm^{-1} and 2929 cm^{-1}, which is attributed to the methyl and imidazole ring of imidazole ligands [37,38]. Besides, the band at 400 cm^{-1} can be assigned to Zn-N and Co-N stretch, demonstrating that Zn^{2+} and Co^{2+} were coordinated with N atom in the imidazole ring, and the structure of the ligand was intact [39]. Compared to FTIR spectra of imidazole ligands (curve a), no characteristic peak was observed at 1845 cm^{-1} and 2648 cm^{-1}, which should belong to N-H-N hydrogen bond absorption and N-H vibration. The disappearance of the two strong bands shows the deprotonation of 2-methyl imidazole in the preparation process. Curve d shows the FTIR spectrum of AuNPs/ZIF-8@ZIF-67. It is known that there are no characteristic peaks for Au in the IR region and the FTIR spectra of AuNPs/ZIF-8@ZIF-67 shows good coherence with that of ZIF-8@ZIF-67 [35].

XRD patterns also authenticated the preparation of ZIF-8, ZIF-8@ZIF-67 and AuNPs/ZIF-8@ZIF-67, as illustrated in Figure 1B. The presence of diffraction peaks with high intensity demonstrated that the synthesized products all had a crystalline

structure. The characteristic peaks at 7.4 °, 10.4 °, 12.3 °, 16.5 °, 18.1 ° and 26.8 ° corresponded to the crystal plane of (011), (002), (112), (013), (222) and (134) belonging to ZIF-8, which is consistent with previous reports [40]. Since ZIF-8 and ZIF-67 have the same topology and approximate unit cell parameters, the synthesized ZIF-8@ZIF-67 should have almost the same spectrum as the parent ZIF-8. As the ZIF-67 shell increased, no structural changes were observed in ZIF-8@ZIF-67, and the skeleton of parent ZIF-8 remained intact during the synthesis [33]. In addition, the sharp peaks appearing at 7.4° and 12.3° indicated that the synthesized ZIF-8@ZIF-67 structure was highly crystalline. Such results were highly similar to the previously reported ZIF-8@ZIF-67 [41]. Shown as curve c in Figure 1B, after encapsulation of AuNPs, the main diffraction peaks of ZIF-8@ZIF-67 remained unchanged, which can be attributed to the small sizes and high dispersion of AuNPs [42].

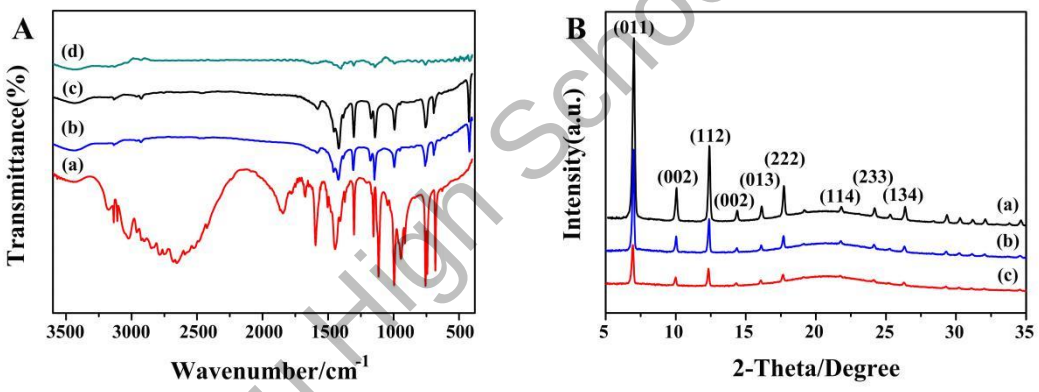

Figure 1. (A) FTIR spectra of (a) 2-MI, (b) ZIF-8, (c) ZIF-8@ZIF-67 and (d) AuNPs/ZIF-8@ZIF-67; (B) XRD patterns of (a) ZIF-8, (b) ZIF-8@ZIF-67 and (c) AuNPs/ZIF-8@ZIF-67.

The core-shell structure and morphology of ZIF-8@ZIF-67 and AuNPs/ZIF-8@ZIF-67 were characterized by TEM and SEM, respectively. As seen in Figure 2A, 2B and 2C, a typical rhombic dodecahedron shape was well preserved in the process of heterogeneous nucleation owing to the similar crystal unit cell and metal-ligand mode, which matches well with XRD result [29,31]. The particle size was found to increase from 358 nm of the ZIF-8 core (Figure 2A) to 425 nm after the ZIF-67 shell growth (Figure 2B). However, after a homogeneous distribution of

AuNPs was observed on the surface of ZIF-8@ZIF-67 (Figure 2C), the particle size of AuNPs/ZIF-8@ZIF-67 decreased to 410 nm and some of the surface seemed to be etched. This might be due to some reaction between ZIF-8@ZIF-67 and $HAuCl_4$ along with the in-situ reduction of $HAuCl_4$ on the surface. Elementary mapping (Figure 2E) further confirmed the core-shell structure of ZIF-8@ZIF-67, which was clearly seen a Zn-containing core and a Co-containing shell. In addition, as shown in the Figure 2F, the EDS peaks corresponding to Co and Zn confirmed the elemental composition of ZIF-8@ZIF-67, and the atomic ratio of Co/Zn was 0.63, which is benefit to form ZIF-8@ZIF-67 core-shell structure [41].

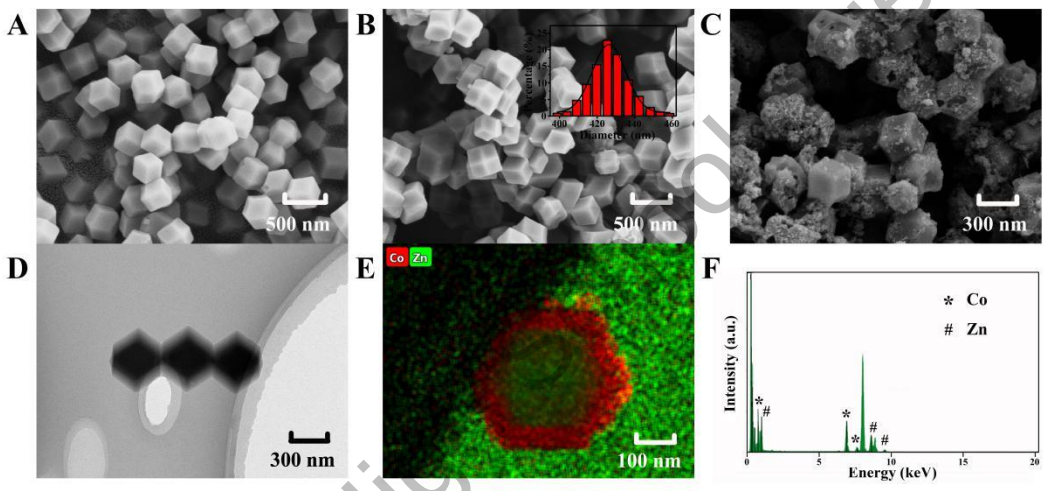

Figure 2. SEM images of the (A) ZIF-8; (B) ZIF-8@ZIF-67 and (C) AuNPs/ZIF-8@ZIF-67. (D) TEM image, (E) elemental mapping and (F) EDS spectrum of ZIF-8@ZIF-67.

3.2 Feasibility of the amplification strategy

In order to characterize the stepwise modification process of the aptasensor, EIS at each immobilization step was recorded as shown in Figure 3A. Curve a represented the impedance spectrum of ITO, with an electron transfer resistance (R_{et}) value around 135.2 Ω. When the AuNPs/ZIF-8@ZIF-67 was modified onto the ITO surface, the diameter of semicircle (curve b) decreased since external AuNPs helped enhance the interface electron transfer. After the modification of HP1 through Au-S bond, R_{et} value

increased from 96.7 to 133.6 Ω (cure c), which can be explained that the negative-charged HP1 electrostatically repulsed the negative-charged electrochemical probe of $[Fe(CN)_6]^{3-/4-}$, decreasing the electron transfer rate from $[Fe(CN)_6]^{3-/4-}$ to electrode surface. A larger semicircle domain was displayed after the electrode was blocked with 0.25 % BSA (curve d). Curve e depicts the hybrization of ssDNA with HP1, by unfolding HP1 from hairpin rigid structure to liner flexible structure, with a very small R_{et} value around 71 Ω. The decrease of R_{et} can be explained in terms of steric effects caused by structural changes of chains. As for electrode treating with HCR, a further increased R_{et} was observed because the exponential negatively charged nucleic acids immobilized onto the sensing interface [43]. According to the characterization of impedance spectra, each step of fabrication was successfully conducted and HCR/ssDNA/HP1/AuNPs/ZIF-8@ZIF-67/ITO was proved to be well assembled. The fitted R_{et} values were calculated based on the equivalent circuit, which consisted of four main elements: electrolyte solution resistance (R_s), R_{et}, the double layer capacitance (C_{dl}) and Warburg impedance (Z_w) (inset part in Figure 3A).

Feasibility of the strategy employed for amplifying signals was verified by DPV with different modified electrodes under diverse detection conditions. Figure 3B illustrated the DPV responses of different aptasensors. Curve a corresponded to ssDNA/HP1/AuNPs/ZIF-8@ZIF-67/ITO electrode in 0.1 M pH 7.0 PBS, in which no visible DPV signals could be seen. It indicated that no electrochemical probe Thi on the electrode surface at this time. After HCR structure formed on the electrode surface, Thi could be electrostatically adsorbed on HCR, arousing a low current response (curve b) mainly due to the insulating nature of oligonucleotides. When hemin/G-quadruplex DNAzyme formed with the participation of hemin, an obviously increased peak current was obtained in the presence of 3.0 mM NADH (curve c) due to the synergistic catalytic effect between DNAzyme and NADH. The obtained current was about 2.6 times of that in curve b, illustrating enhanced signal amplification. For comparison, in the presence of 1 pg mL^{-1} target OTA, a weaker DPV signal (cure d) was recorded since the strong affinity between HP and OTA caused less ssDNA was released.

To further evaluate the feasibility of the aptasensor, polyacrylamide gel electrophoresis (PAGE) analysis was conducted by DNA electrophoresis on various stages of samples [44]. As shown in Figure 3C, lane 1 to 4 corresponded to HP, HP1, HP2 and HP3, and four bright bands could be observed respectively. In the absence of OTA, HP hybridized with RNA which gave a good explanation for a bright band in lane 5, and the height was a little higher than that of HP. After adding DSN in duplex HP/RNA, HP was digested while ssDNA was released. No obvious band was observed in lane 6 which might be explained by the fact that single-stranded ssDNAs with much smaller molecular weights were hard to detected in electrophoresis analysis. Lane 7 and 8 corresponded to ssDNA/HP1 and ssDNA/HP1/HCR, two bright bands illustrated the hybridization among ssDNA, HP1, AP, HP2 and HP3 was successful. In addition, lane 7 was found to be a little higher than lane 2, which can be attributed to the combination of ssDNA and HP1. Lane 8 was the highest band in this image, illustrating the large molecule nature of HCR structure. Therefore, the PAGE result fully confirmed the strong interactions among these sequences and the feasibility of the sensing strategy in this work.

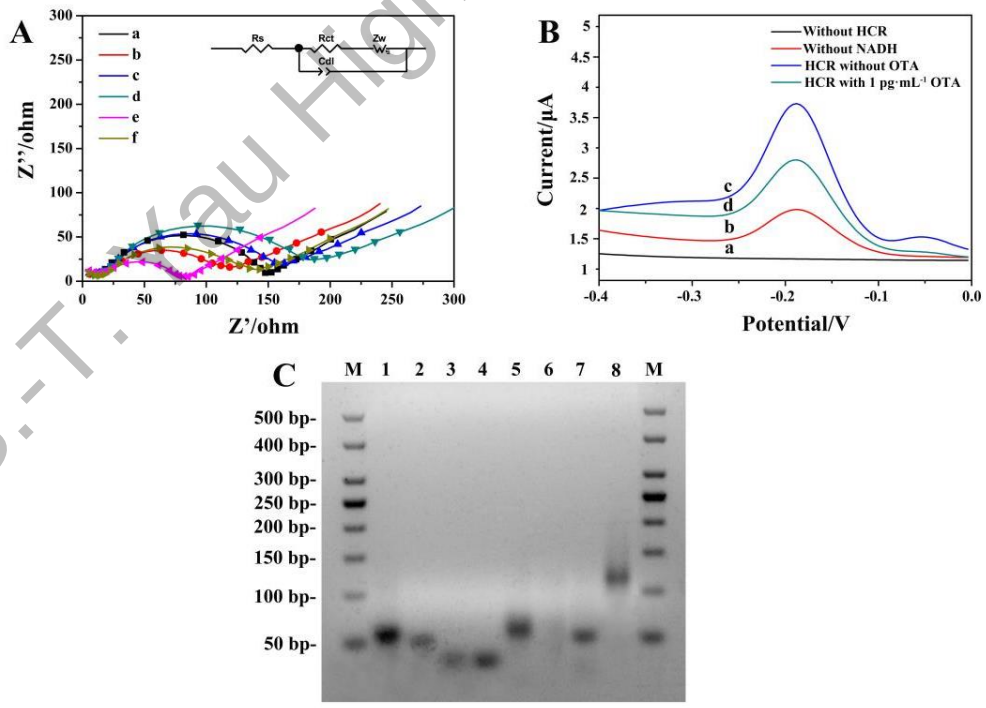

Figure 3. (A) Nyquist plots of different modified electrodes were recorded in 0.1 M pH 7.0 PBS containing 5.0 mM $[Fe(CN)_6]^{3-/4-}$: (a) bare ITO, (b)

AuNPs/ZIF-8@ZIF-67/ITO, (c) HP1/AuNPs/ZIF-8@ZIF-67/ITO, (d) BSA/HP1/AuNPs/ZIF-8@ZIF-67/ITO, (e) ssDNA/HP1/AuNPs/ZIF-8@ZIF-67/ITO, (f) HCR/ssDNA/HP1/AuNPs/ZIF-8@ZIF-67/ITO. (B) The corresponding DPV signals of aptasensors in 0.1 M pH 7.0 PBS (a) blank (without HCR), (b) HCR in the absence of NADH, (c) HCR in the presence of NADH, (d) HCR in the presence of NADH with 1 pg·mL^{-1} target OTA. (C) The PAGE analysis: lane 1-4 corresponded to HP, HP1, HP2 and HP3, respectively; lane 5 and 6 corresponded to HP/RNA and HP/RNA/DSN; lane 7 and 8 corresponded to ssDNA/HP1 and ssDNA/HP1/HCR, respectively; lane M was the DNA marker.

3.3 Kinetic study of the modified electrode

In order to study the kinetic principle of the electrochemical process, CV curves were recorded at different scan rates (ν) from 10 to 150 mV·s^{-1}. As shown in Figure 4A, CV curves dispalyed a good symmetry at different scanning rates accompanying with a significant pair of redox peaks, in which $[Fe(CN)_6]^{3-/4-}$ worked as the oxidation-reduction probe. By deducing the relationship between redox peak currents and the square root of scan rate ($\nu^{1/2}$), a linear relationship can be acquired, indicating a diffusion controlled electrochemical process. It meant that a fast electron transfer between the $Fe(CN)_6^{4-}$ and the electrode surface, demonstrating an excellent conductivity of AuNPs/ZIF-8@ZIF-67 and a uniform distribution of AuNPs in pores of ZIF-8@ZIF-67 (Figure 4B).

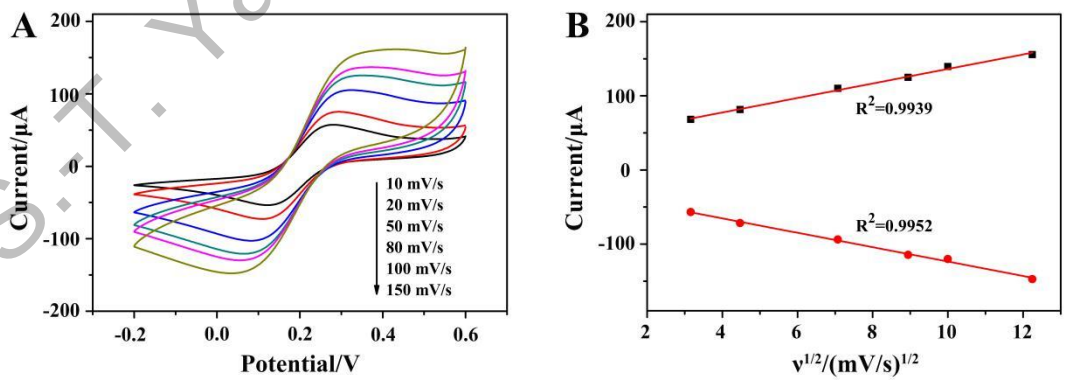

Figure 4. (A) CVs of HP1/AuNPs/ZIF-8@ZIF-67/ITO at the scan rate of 10, 20, 50, 80, 100 and 150 mV·s^{-1} (from internal to external) in 0.1 M PBS solution containing

5.0 mM $[Fe(CN)_6]^{3-/4-}$, respectively. (B) The corresponding plot of peak current vs. $\nu^{1/2}$.

3.4 Optimization of experimental parameters

To improve the performance of the aptasensor, the reaction parameters of HP1 concentration, DSN dosage, DSN cleaving temperature and reaction time were investigated by EIS and DPV [45-47]. As shown in Figure 5A, along with the concentration of HP1 increased from 0 to 2.4 μM, the detected R_{et} value of HP1/AuNPs/ZIF-8@ZIF-67/ITO increased accordingly and the largest value appeared at 1.6 μM. If the immobilized HP1 exceeded 1.6 μM, the R_{et} value seemed decreased a little, which might be ascribed that excessive HP1 could not link the limited active sites on AuNPs/ZIF-8@ZIF-67/ITO surface. It meant that 1.6 μM dosage of HP1 was saturated for electrode modification, and selected as the optimal concentration.

DSN could cleave HP in heteroduplex of HP/RNA and thus release the RNA strand for amplification cycle. The reaction temperature, time and DSN dosage are important for the optimal performance of DSN catalytic reaction, which should be studied and discussed. In this experiment, thiolated-HP was firstly immobilized onto an Au electrode (AuE) through Au-S by incubating with 20 μL of 2 μM HP for 2 h. After rinsing with 0.1 M PBS (pH 7.0), the R_{et} value of HP/AuE (R_{et1}) was detected. Then, 10 μL of reaction solution composed of 8 μL PBS, 1 μL master buffer, 1 μL 2 μM RNA and 0.1 μL DSN with different contents was immersed on HP/AuE surface at different reaction time and temperature. During the reaction, a part of HP could be digested and released from electrode surface, and the R_{et} value would decrease (R_{et2}). The results were shown in Figure 5B to D, the ordinate of reaction rate (%) was calculated as the ratio between R_{et} change ($\Delta R_{et} = R_{et1} - R_{et2}$) and R_{et1}, which was varied by the reaction temperature, time and dosage. As a result, the optimal experimental conditions were selected as 50 ℃, 30 min and 0.2 U.

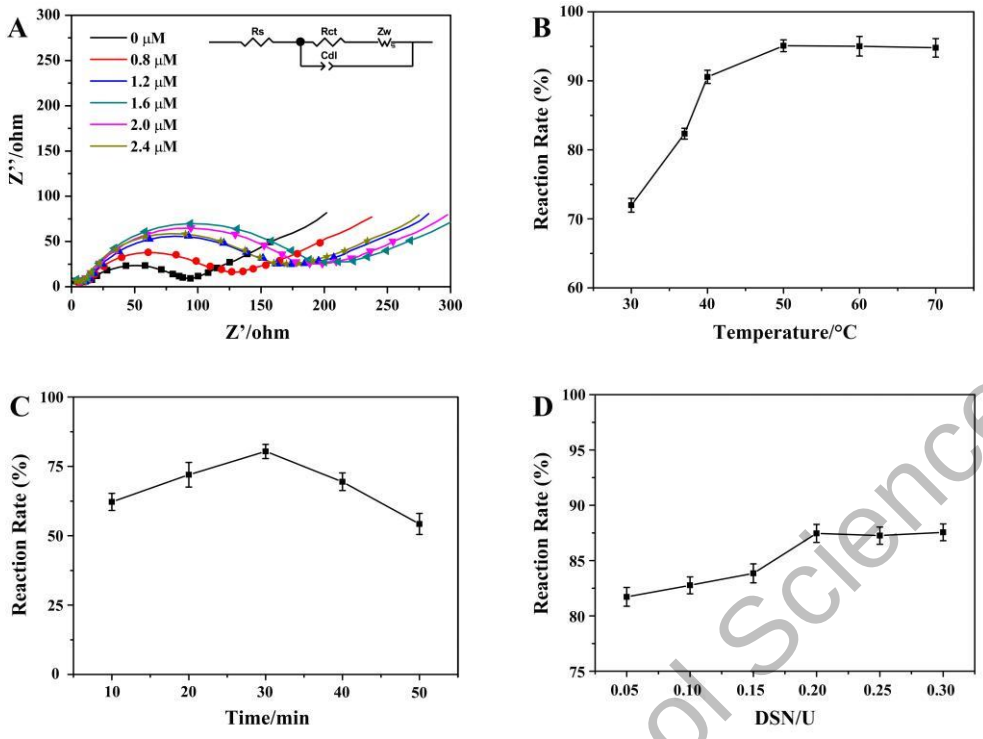

Figure 5. (A) Nyquist plots of HP1/AuNPs/ZIF-8@ZIF-67/ITO immobilized with different concentrations of HP1 recorded in 0.1 M pH 7.0 PBS containing 5.0 mM $[Fe(CN)_6]^{3-/4-}$. Effects of DSN reaction rate (%) on (B) reaction temperature, (C) reaction time and (D) DSN dosage, respectively.

3.5 Electrocatalytic performance of the aptasensor

Under the optimal conditions, the performance of the aptasensor was evaluated in terms of sensitivity and dynamic response range. In the absence of OTA, the DPV current of Thi was recorded as I_0. In the presence of OTA, the high infinity of OTA with its aptamer led to the decrease in the amount of HP/RNA, and thus the corresponding current response of Thi (I) became lower. A gradual reduction of DPV current was observed as adding OTA from 1 fg·mL^{-1} to 10 ng·mL^{-1} (Figure 6A). As shown in Figure 6B, a good linearity between the peak current change ($\Delta I_p = I_0$-I) and the logarithm of OTA concentration is obtained, with a linear equation of $\Delta I_p/\mu A$= 0.14logC/fg·mL^{-1}+1.25 (n=5, R^2=0.9923). The limit of detection was evaluated to be 0.247 fg·mL^{-1} according to 3 σ principle. Compared with the performance of previous

reported OTA aptasensors, as listed in Table 2, the proposed aptasensor exhibited a wide linear range by eight orders of magnitude with a low detection limit. The advantages of our work were ascribed to six aspects: (1) the controllable and perfect core-shell structured ZIF-8@ZIF-67 provided rich active sites and a large surface area for DNA strands modification; (2) the in-situ implantation of AuNPs significantly enhanced the electron transfer rate; (3) DSN was used for selective digestion of DNA strand in DNA/RNA hybrid, providing a good chance for designing a RNA recycled amplification strategy; (4) the G-quadruplex-hemin assembled HCR nanowire acted as an NADH oxidase to assist the concomitant formation of H_2O_2 in the presence of dissolved O_2; (5) meanwhile, the G-quadruplex-hemin assembled HCR nanowire acted as an HRP-mimicking DNAzyme to catalyze the reduction of the produced H_2O_2; (6) With the redox probe Thi as electron mediator, the pseudobienzyme electrocatalytic system combined with the aptamer recognition strategy endowed a dramatically amplified electrochemical aptasensing performance.

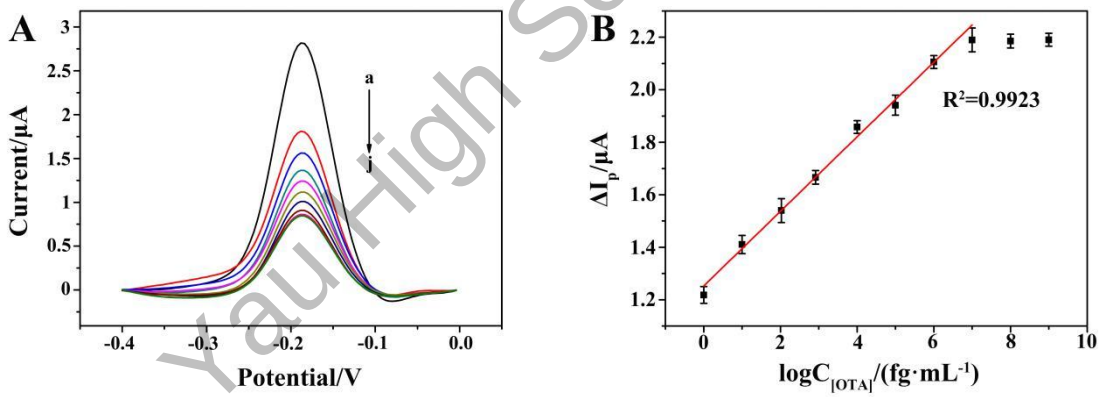

Figure 6. (A) DPV responses at the HCR/ssDNA/HP1/AuNPs/ZIF-8@ZIF-67/ITO with varying concentrations of OTA from 1 fg·mL^{-1} to 10 ng·mL^{-1} (curve a to j). (B) Linear relationship between the peak current change and the logarithm of OTA concentration from 1 fg·mL^{-1} to 10 ng·mL^{-1}.

Table 2. Performance comparisons of different OTA aptasensors

Sensor category	Method	Liner range (pg/mL)	Detection limit (pg/mL)	Ref.
Optical method	Colorimetry	1009.5-4038	1009.5	[48]
	DNA hydrogel	50-10^5	10	[49]
	SPR	10^{-3}-100	2.5×10^{-4}	[50]
Electrochemistry	SWV	1-10^5	0.7	[51]
	Chemiluminescence	10-10^5	4.28	[52]
	Chronoamperometry	1-20	0.4	[53]
	DPV	1-10^3	0.5	[54]
	DPV	10^{-3}-10^5	0.247	This work

3.6 OTA detection in real samples

To further verify the performance of the aptasensor in the detection of OTA in real samples, three OTA solutions with the concentrations of 1.0, 5.0 and 10.0 pg·mL^{-1} were spiked into the wheat sample extract. 5 g wheat flour was added into 20 mL of acetonitrile-water (v/v = 9:1) and treated with ultrasonic wave for 20 min. After centrifugation and filtration, the supernatant was ready for use. As shown in Table 3, the recoveries of these detections were in the range of 96.8-104.2 % with the relative standard derivations (RSD) values of 3.0-5.9 %. According to the experimental results, our assay was applicable for quantitative determination of OTA in real samples with enough precision and accuracy.

Table 3. Detection results of wheat samples spiked with OTA.

OTA Sample	Added	Found	Recovery(%)	RSD(%)
1	1.0 pM	0.998 pM	99.8	1.6
2	5.0 pM	4.84 pM	96.8	5.9
3	10.0 pM	10.42 pM	104.2	3.0

4. Conclusion

In conclusion, we have designed a highly sensitive OTA aptasensor by conducting an enzymatic signal amplification system, accompanying with core-shell ZIF-8@ZIF-67 materials and the autonomously assembled hemin/G-quadruplex DNAzyme for further signal amplification. In this article, ZIF-8@ZIF-67 provided abundant available functional groups for subsequent modification of AuNPs, which is in favor of immobilization of HP1 on AuNPs/ZIF-8@ZIF-67/ITO electrode. Owing to the specific ability of DSN to identify and cleave DNA from DNA/RNA heteroduplex, ssDNA thus could be released and to open HP1 assembled on the electrode, which successfully triggered the HCR and further realized the pseudobienzyme electrocatalytic amplification. This constructed aptasensor exhibited a high sensitivity from 1 fg·mL^{-1} to 10 ng·mL^{-1} and a low detection limit of 0.247 fg·mL^{-1}. Furthermore, the aptasensor was proven to be applied in wheat samples which demonstrated the potential prospects in practical detection.

Acknowledgements

This work was financially supported by the National Key Research and Development Program (2017YFC1600604), National Natural Science Foundation of China (21575064).

References

[1] H. J. Lee, D. Ryu, Worldwide occurrence of mycotoxins in cereals and cereal-derived food products: public health perspectives of their co-occurrence, J. Agr. Food Chem. 2016, 65, 7034-7051.

[2] N. Nekrasov, D. Kireev, A. V. Emelianov, I. Bobrinetskiy, Graphene-based sensing platform for on-chip ochratoxin A detection, Toxins, 2019, 11, 550.

[3] B. Han, C. Fang, L. J. Sha, M. Jalalah, M. S. Al-Assiric, F. A. Harraz, Y. Cao, Cascade strand displacement reaction-assisted aptamer-based highly sensitive detection of ochratoxin A, Food Chem. 2021, 338, 127827.

[4] C. X. Gu, L. Y. Yang, M. H. Wang, N. Zhou, L. H. He, Z. H. Zhang, M. Du, A bimetallic (Cu-Co) Prussian blue analogue loaded with gold nanoparticles for impedimetric aptasensing of ochratoxin A, Microchim. Acta 2019, 186, 343.

[5] C. Giovannoli, C. Passini, F. Di Nardo, L. Anfossi, C. Baggiani, Determination of ochratoxin A in Italian red wines by molecularly imprinted solid phase extraction and HPLC analysis, J. Agr. Food Chem. 2014, 62, 5220-5225.

[6] D. E. Armstrong-Price, P. S. Deore, R. A. Manderville, Intrinsic “turn-on” aptasensor detection of ochratoxin A using energy-transfer fluorescence. J. Agr. Food Chem. 2020, 68, 2249-2255.

[7] K. Zhang, M. R. Schaab, G. Southwood, E. R. Tor, L. S. Aston, W. Song, B. Eitzer, S. Majumdar, T. Lapainis, H. Mai, K. Tran, A. El-Demerdash, V. Vega, Y. Cai, J. W. Wong, A. J. Krynitsky, T. H. Begley, A collaborative study: determination of mycotoxins in corn, peanut butter, and wheat flour using stable isotope dilution assay (SIDA) and liquid chromatography-tandem mass spectrometry (LC-MS/MS). J. Agr. Food Chem. 2016, 65, 7138-7152.

[8] A. Pittet, D. Royer, Rapid, low cost thin-layer chromatographic screening method for the detection of ochratoxin A in green coffee at a control level of 10 μg/kg. J. Agr. Food Chem. 2002, 50, 243-247.

[9] Z. Sun, J. Lv, X. Liu, Z. Tang, X. Wang, Y. Xu, B. D. Hammock, Development of a nanobody-AviTag fusion protein and its application in a streptavidin–

biotin-amplified enzyme-linked immunosorbent assay for ochratoxin A in cereal, Anal. Chem. 2018, 90, 10628-10634.

[10] H. Duan, X. Huang, Y. Shao, L. Zheng, L. Guo, Y. Xiong, Size-dependent immunochromatographic assay with quantum dot nanobeads for sensitive and quantitative detection of ochratoxin A in corn, Anal. Chem. 2017, 89, 7062-7068.

[11] A. Jodra, M. Hervás, M. Á. López, A. Escarpa, Disposable electrochemical magneto immunosensor for simultaneous simplified calibration and determination of Ochratoxin A in coffee samples, Sens. Actuat. B, 2015, 221, 777-783.

[12] M. Bougrini, A. Baraket, T. Jamshaid, A. El Aissari, J. Bausells, M. Zabala, N. El Bari, B. Bouchikhi, N. Jaffrezic-Renault, E. Abdelhamid, N. Zine, Development of a novel capacitance electrochemical biosensor based on silicon nitride for ochratoxin A detection, Sens. Actuat. B, 2016, 234, 446-452.

[13] N. Hao, Z. Dai, M. Xiong, R. Hua, J. W. Lu, K. Wang, A portable solar-driven ratiometric photo-electrochromic visualization biosensor for detection of ochratoxin A, Sens. Actuat. B, 2020, 306, 127594.

[14] H. F. Zhang, Z. S. Zhuo, L. J. Chen, C. Q. Chen, F. Luo, Y. T. Chen, L. H. Guo, B. Qiu, Z. Y. Lin, G. N. Chen, Enhanced performance of a hyperbranched rolling circle amplification based electrochemiluminescence aptasensor for ochratoxin A using an electrically heated indium tin oxide electrode, Electrochem. Commun. 2018, 88, 75-78.

[15] M. Wei, S. Yue, Y. Liu, An amplified electrochemical aptasensor for ochratoxin A based on DNAzyme-mediated DNA walker, J. Electroanal. Chem. 2021, 891, 115269.

[16] S. Dai, S. Wu, N. Duan, J. Chen, Z. Zheng, Z. Wang, An ultrasensitive aptasensor for ochratoxin A using hexagonal core/shell upconversion nanoparticles as luminophores, Biosens. Bioelectron. 2017, 91, 538-544.

[17] J. A. Cruz-Aguado, G. Penner, Determination of ochratoxin A with a DNA aptamer, J. Agr. Food Chem. 2008, 56, 10456-10461.

[18] J. Zhang, J. Chen, X. Zhang, Z. Zeng, M. Chen, S. Wang, An electrochemical biosensor based on hairpin-DNA aptamer probe and restriction endonuclease for Ochratoxin A detection, Electrochem. Commun. 2012, 25, 5-7.

[19] Y. Yang, Y. Zhou, Y. Xing, G. Zhang, Y. Zhang, C. Zhang, P. Lei, C. Dong, X. Deng, Y. He, S. Shuang, A label-free aptasensor based on aptamer/NH_2 Janus particles for ultrasensitive electrochemical detection of ochratoxin A, Talanta, 2019, 199, 310-316.

[20] Z. Tang, Z. Ma, Multiple functional strategies for amplifying sensitivity of amperometric immunoassay for tumor markers: a review, Biosens. Bioelectron. 2017, 98, 100-112.

[21] J. Yu, C. Mu, B. Yan, X. Qin, C. Shen, H. Xue, H. Pang, Nanoparticle/MOF composites: preparations and applications, Mater. Horizons 2017, 4, 557-569.

[22] F. Yi, D. Chen, M. Wu, L. Han, H. Jiang, Chemical sensors based on metal-organic frameworks, Chem. Plus Chem. 2016, 81, 675-690.

[23] Y. Pan, S. Zhan, F. Xia, Zeolitic imidazolate framework-based biosensor for detection of HIV-1 DNA, Anal. Biochem. 2018, 546, 5-9.

[24] L. Dai, Y. Li, Y. Wang, X. Luo, D. Wei, R. Feng, T. Yan, X. Ren, B. Du, Q. Wei, A prostate-specific antigen electrochemical immunosensor based on Pd NPs functionalized electroactive Co-MOF signal amplification strategy, Biosens. Bioelectron. 2019, 132, 97-104.

[25] C. P. Guo, M. Y. Hu, Z. Z. Li, F. H. Duan, L. H. He, Z. H. Zhang, F. Marchetti, M. Du, Structural hybridization of bimetallic zeolitic imidazolate framework (ZIF) nanosheets and carbon nanofibers for efficiently sensing α-synuclein oligomers, Sens. Actuat. B, 2020, 309, 127821.

[26] H. N. Abdelhamid, Hierarchical porous ZIF-8 for hydrogen production via the hydrolysis of sodium borohydride, Dalton Trans. 2020, 49, 4416-4424.

[27] M. Eddaoudi, D. F. Sava, J. F. Eubank, K. Adil, V. Guillerm, Zeolite-like metal-organic frameworks (ZMOFs): design, synthesis, and properties, Chem. Soc. Rev. 2015, 44, 228-249.

[28] R. Banerjee, A. Phan, B. Wang, C. Knobler, H. Furukawa, M. O'Keeffe, O. M. Yaghi, High-throughput synthesis of zeolitic imidazolate frameworks and application to CO_2 capture, Science 2008, 319, 939-943.

[29] Y. H. Zhou, X. Y. Cao, J. Z. Ning, C. C. Ji, Y. Cheng, J. Gu, Pd-doped Cu

nanoparticles confined by ZIF-67@ZIF-8 for efficient dehydrogenation of ammonia borane, Int. J. Hydrogen Ener. 2020, 45, 31440-31451.

[30] D. K. Panchariya, R. K. Rai, E. A. Kumar, S. K. Singh, Core-shell zeolitic imidazolate frameworks for enhanced hydrogen storage, ACS Omega 2018, 3, 167-175.

[31] X. P. Qiu, H. Zhang, H. L. Yu, T. L. Jiang, Y. Luo, Duplex-specific nuclease-mediated bioanalysis, Trend. Biotech., 2015, 33, 180-188.

[32] H. J. Qi, S. Z. Yue, S. Bi, W. L. Song, A versatile homogeneous chemiluminescence biosensing platform based on exonuclease-assisted hybridization chain reaction, Sens. Actuat. B, 2018, 273, 1525-1531.

[33] Y. Pan, K. A. Sun, S. J. Liu, X. Cao, K. L. Wu, W. C. Cheong, Z. Chen, Y. Wang, Y. Li, Y. Q. Liu, D. S. Wang, Q. Peng, C. Chen, Y. D. Li, Core-shell ZIF-8@ZIF-67-derived CoP nanoparticles-embedded N-doped carbon nanotube hollow polyhedron for efficient over-all water splitting, J. Am. Chem. Soc. 2018, 140, 2610-2618.

[34] X. C. Lan, N. Huang, J. F. Wang, T. F. Wang, A general and facile strategy for precisely controlling the crystal size of monodispersed metal-organic frameworks via separating the nucleation and growth, Chem. Commun. 2018, 54, 584-587.

[35] Y. Wang, X. Li, G. I. N. Waterhouse, Y. L. Zhou, H. S. Yin, S. Y. Ai, Photoelectrochemical biosensor for protein kinase A detection based on carbon microspheres, peptide functionalized Au-ZIF-8 and TiO_2/g-C_3N_4. Talanta, 2019, 196, 197-203.

[36] Y. L. Yuan, M. Gao, G. P. Liu, Y. Q. Chai, S. Q. Wei, R. Yuan, Sensitive pseudobienzyme electrocatalytic DNA biosensor for mercury(II) ion by using the autonomously assembled hemin/G-quadruplex DNAzyme nanowires for signal amplification, Anal. Chim. Acta 2014, 811, 23-28.

[37] J. Yang, F. J. Zhang, H. Y. Lu, X. Hong, H. L. Jiang, Y. E. Wu, Y. D. Li, Hollow Zn/Co ZIF particles derived from core-shell ZIF-67@ZIF-8 as selective catalyst for the semi-hydrogenation of acetylene, Angew. Chem. 2015, 127, 11039-11043.

[38] Z. Zhang, S. Xian, H. Xi, H. Wang, Z. Li, Improvement of CO_2 adsorption on

ZIF-8 crystals modified by enhancing basicity of surface, Chem. Engin. Sci. 2011, 66, 4878-4888.

[39] Z. H. Zhang, J. L. Zhang, J. M. Liu, Z. H. Xiong, C. Xu, Selective and competitive adsorption of azo dyes on the metal-organic framework ZIF-67, Water Air Soil Poll. 2016, 227, 471.

[40] K. S. Park, Z. Ni, A. P. Cote, J. Y. Choi, R. D. Huang, F. J. Uribe-Romo, H. K. Chae, M. O'Keeffe, O. M. Yaghi, Exceptional chemical and thermal stability of zeolitic imidazolate frameworks, P. Natl. Acad. Sci. USA, 2006, 103, 10186-10191.

[41] A. T. Gu, J. Y. Chen, Q. H. Gao, M. M. Khan, P. Wang, Y. Jiao, Z. X. Zhang, Y. Liu, Y. Yang, The preparation of Ag/ZIF-8@ZIF-67 core-shell composites as excellent catalyst for degradation of the nitroaromatic compounds, Appl. Surf. Sci. 2020, 516, 146160.

[42] Y. J. Zhang, Q. Z. Li, C. X. Liu, X. G. Shan, X. Chen, The promoted effect of a metal-organic frameworks (ZIF-8) on Au/TiO_2 for CO oxidation at room temperature both in dark and under visible light irradiation, Appl. Catal. B 2018, 224, 283-294.

[43] X. Y. Wang, Y. Q. Shan, Gong M, X. Jin, A novel electrochemical sensor for ochratoxin A based on the hairpin aptamer and double report DNA via multiple signal amplification strategy, Sens. Actuat. B 2019, 281, 595-601.

[44] Z. B. Li, N. Xue, H. Y. Ma, Z. Y. Cheng, X. M. Miao, An ultrasensitive and switch-on platform for aflatoxin B1 detection in peanut based on the fluorescence quenching of graphene oxide-gold nanocomposites, Talanta 2018, 181, 346-351.

[45] G. Huang, J. Ouyang, J. R. Delanghe, W. R. G. Baeyens, Z. Dai, Chemiluminescent image detection of haptoglobin phenotyping after polyacrylamide gel electrophoresis, Anal. Chem. 2004, 76, 2997-3004.

[46] X. Sun, H. Chen, S. Wang, Y. Zhang, Y. Tian, N. Zhou, Electrochemical detection of sequence-specific DNA based on formation of G-quadruplex-hemin through continuous hybridization chain reaction, Anal. Chim. Acta 2018, 1021, 121-128.

[47] H. Zhang, M. Fan, J. Jiang, Q. Shen, C. Cai, J. Shen, Sensitive electrochemical biosensor for microRNAs based on duplex-specific nuclease-assisted target recycling followed with gold nanoparticles and enzymatic signal amplification, Anal. Chim.

Acta 2019, 1064, 33-39.

[48] C. Liu, Y. J. Guo, F. Luo, P. F. Rao, C. L. Fu, S. Y. Wang, Homogeneous electrochemical method for ochratoxin A determination based on target triggered aptamer hairpin switch and exonuclease III-assisted recycling amplification, Food Anal. Method. 2017, 10, 1982-1990.

[49] L. L. Hao, W. Wang, X. Q. Shen, S. L. Wang, Q. Li, F. L. An, S. J. Wu, A fluorescent DNA hydrogel aptasensor based on the self-assembly of rolling circle amplification products for sensitive detection of ochratoxin A, J. Agr. Food Chem. 2019, 68, 369-375.

[50] X. B. Huang, S. H. Wu, H. C. Hu, J. J. Sun, AuNanostar@4-MBA/AuNPs core-shell nanostructure coupled with exonuclease III-assisted cycling amplification for ultrasensitive SERS detection of ochratoxin A, ACS Sensor. 2020, 5, 2636-2643.

[51] A. Suea-Ngam, P. D. Howes, C. E. Stanley, A. J. Demello, An exonuclease I-assisted silver-metallized electrochemical aptasensor for ochratoxin A detection, ACS Sensors, 2019, 4, 1560-1568.

[52] P. Shen, W. Li, Y. Liu, Z. Ding, Y. Deng, X. R. Zhu, Y. H. Jin, Y. C. Li, J. L. Li, T. S. Zheng, High-throughput low-background G-quadruplex aptamer chemiluminescence assay for ochratoxin a using a single photonic crystal microsphere, Anal. Chem. 2017, 89, 11862-11868.

[53] J. Zhang, J. H. Chen, Zhang X, Z. G. Zeng, M. Chen, S. H. Wang, An electrochemical biosensor based on hairpin-DNA aptamer probe and restriction endonuclease for ochratoxin A detection, Electrochem. Commun. 2012, 25, 5-7.

[54] X. Wang, Y. Shan, M. Gong, X. Jin, L. Lv, M. Jiang, J. Xu, A novel electrochemical sensor for ochratoxin A based on the hairpin aptamer and double report DNA via multiple signal amplification strategy, Sens. Actuat B 2019, 281, 595-601.

致谢页

本论文得到了国家重点研发计划课题（2017YFC1600604）及国家自然科学基金项目（21575064）的大力支持。

我们是一群对化学有着浓厚兴趣的高中生。我们很幸运很珍惜能够参加这个科研项目，通过一年多的努力，我们顺利完成了项目并参加丘成桐中学科学奖的比赛。这一路走来有苦有泪更有感激和收获。

首先感谢南京工业大学的陈晓君教授及其团队在百忙之中无偿帮我们调整实验思路，教我们实验方法，教我们数据的分析及结果的分析。感谢指导教师南京外国语学校陈静老师无偿给予的指导与支持，在我们实验困难的时候给我鼓励，帮我们想办法解决。感谢陈静老师指引我们走入探索之路，教会我学习和科研如何兼得，搞好科研的同时不能耽误学校课程。我们还要感谢我们的学校南京外国语学校，感谢优秀的学校平台提供给我科研的宝贵机会，这在一般的高中是不可能有的机会。我们三位队员分工明确，紧密合作。丁冠文负责文献资料收集和整理、参与设计实验方案，负责核壳 ZIFs 材料制备与表征，及其性能测试；夏锐涵负责电化学适配体传感器的构建，可行性分析及性能测试；杨博约负责传感器稳定性、特异性等表征，实际样品检测以及数学建模计算。丁冠文负责论文初稿撰写工作，夏锐涵负责数据整理和作图，杨博约负责文献整理。我们三人共同参与了文章修改工作。

主要完成人：

丁冠文，男，18 岁，南京外国语学校高三学生，对化学和生物兴趣浓厚，围绕生化方向积极开展活动，并获得如下成绩：

（1）2021 年美国生物奥赛铜奖

（2）2021 年英国生物奥赛铜奖

（3）2020 年 IGEM 全球金奖

（4）2020 年全国中学生生物学联赛江苏省二等奖

（5）2020 年以共同作者发表 SCI 生物论文 1 篇

（6）获得 2 个实用新型专利

夏锐涵，男，18 岁，南京外国语学校高三学生，担任南京外国语学校美式辩

论社社长、南京外国语学校学生会主席。平时兴趣爱好广泛，并获得以下成绩：

（1）“随园杯”物理竞赛二等奖；

（2）时代杯数学竞赛一等奖；

（3）ARML 数学竞赛团体银奖，全球 TOP100；

（4）NSDA 辩论赛南京赛区一等奖；

（5）TOC 全国赛优秀辩手

杨博约，男，17 岁，就读于南京外国语学校高三，对数理化类学科兴趣浓厚，并取得过以下成绩：

（1）AMC12 全球优秀奖

（2）HIMCM finalist 奖

（3）ARML Power 全国金奖

（4）在物理碗、IEO、IOC 等竞赛中也有所斩获

指导老师：

陈晓君，女，南京工业大学化学与分子工程学院教授、博士生导师、江苏省“青蓝工程”中青年学科带头人、江苏省“六大人才高峰”高层次人才、牛津大学访问学者。研究方向为新型纳米结构组装、光/电化学生物传感、临床分析新方法和食品安全防控新技术。近 5 年来，发表 SCI 论文 50 余篇。主持国家重点研发计划课题、国家自然基金面上项目、江苏省自然基金面上项目等科研项目。

陈静，女，南京外国语学校，中学高级教师，第九届南京市优秀青年教师。教学业务扎实，在省市范围内开设过多节公开课和讲座等，在多项国家以及省市教学竞赛中获奖。科研能力强，主持或参与过多项国家、省以及市级课题；发表十余篇论文，其中 SCI 论文 1 篇，全国中文核心期刊 5 篇。主要研究方向为新课程教学实践、STEM 化学教学等。在 2016 年 “全国基础教育化学新课程实施成果”评选活动中，获一等奖；带领中学生参加 STEM 化学项目研究，获 2017 年丘成桐中学科学奖（化学）全国银奖；在 2020 年江苏省基础教育青年教师教学基本功大赛（高中化学）中获一等奖。